THE ASTROPHYSICAL JOURNAL, 394:174–183, 1992 July 20

COSMIC-RAY SECONDARY ANTIPROTONS: A CLOSER LOOK

THOMAS K. GAISSER AND ROBERT K. SCHAEFER
Bartol Research Institute, University of Delaware, Newark, DE 19716
Received 1991 August 21; accepted 1992 January 29

ABSTRACT

Following a suggestion of Webber that early calculations underestimated the intensity of secondary antiprotons, we have systematically reexamined three aspects of the calculation: the normalization and shape of the present interstellar spectrum, nuclear enhancement of antiproton production in collisions involving nuclei, and the mean energy-dependent residence time of secondary nuclei and antiprotons in the Galaxy. In particular, we have a new estimate of the nuclear enhancement factor, based on the wounded nucleon model. Here we find that the presence of heavy nuclei in the cosmic rays increases the antiproton flux by only 20% over a pure proton composition. We conclude that the reported experimental values of the antiproton-to-proton ratio of $E_p \sim 6$–12 GeV remain significantly above the range of theoretical expectation allowed by uncertainties in the input assumptions.

Subject headings: cosmic rays — elementary particles

1. INTRODUCTION

Antiprotons offer an interesting probe of cosmic-ray propagation models that is complementary to information provided by secondary nuclei such as lithium, beryllium, and boron or the secondaries of iron. Although antiprotons are generated by collisions with interstellar matter just as secondary nuclei are, the details of the production process are in some ways very different. Unlike the spallation cross sections that determine the observed ratios of nuclei, the cross section for $\bar{p}$ production has a high threshold (6 GeV nucleon^{-1} kinetic energy), and it increases rapidly for more than two decades in energy. In addition, unlike secondary nuclei, antiprotons reflect primarily the propagation history of the (dominant) proton component of the cosmic radiation, which could, in principle, be different from that of heavy nuclei.

Secondary cosmic rays are produced when primary cosmic rays collide with interstellar gas as the primaries diffuse from their sources through the turbulent magnetic fields of the Galaxy. The observed intensities of the secondaries depend both on their production rate and on their subsequent diffusion in the galaxy. Since observations are made at 1 AU, the observed fluxes also depend in an important way on solar modulation as the particles diffuse into the inner solar system.

After briefly reviewing the procedure for calculating the secondary fluxes, we proceed to reexamine the normalization and shape of the primary spectrum and the residence time or pathlength parameter, which characterizes the propagation of secondaries after they are produced. We next consider the small but nonnegligible presence of nuclei as projectiles and targets, both of which affect the production rate of secondaries. We use the "wounded" nucleon model to scale nuclear multiplicities to those in the proton-proton collision. Webber & Potgieter (1989) argue that all these effects have been wrongly estimated in previous calculations, in a direction that underestimates the secondary antiproton flux. We assess the range of uncertainty for each factor in the calculation and evaluate how it propagates through to the expected antiproton flux. Our conclusion is that there remains a significant discrepancy with present measurements of antiprotons with energies of 6–12 GeV. The major source of difference between our result and that of Webber & Potgieter is the nuclear enhancement factor, which turns out to be significantly smaller than the one they used. The major remaining uncertainty in interpretation of measurements of antiprotons as a probe of cosmic-ray propagation is the effect of solar modulation. We compare our calculated $\bar{p}$ flux to data in two ways: (1) we compare the predicted interstellar flux to Perko's (1992) demodulated fluxes, and (2) we modulate the antiproton fluxes to get a modulated $\bar{p}/p$ ratio at 1 AU.

2. FACTORS IN THE CALCULATION OF THE SECONDARY $\bar{p}$ FLUX

We begin with the general equations for secondary particle production and propagation in the Galaxy and later specialize to the antiproton case. In this way we hope to emphasize the generality of our antiproton flux result, which holds in a disk-halo diffusion model as well as in the standard leaky box model.

The number density of secondary cosmic rays per unit energy interval $N_s(E)$ in the Galaxy can be calculated from the stationary solution of the continuity equation, i.e., $\partial N_s/\partial t = 0$:

$$\frac{\partial}{\partial t} N_s(E, \boldsymbol{r}) = 0 = Q_s(E, \boldsymbol{r}) - \nabla \cdot [(\boldsymbol{u} - D\nabla) N_s(E, \boldsymbol{r})] - \frac{1}{\tau_i} N_s(E, \boldsymbol{r}) - \frac{\partial}{\partial E} b(E) N_s(E, \boldsymbol{r}) \,. \quad (1)$$

The first term on the right-hand side of the equation is $Q_s(E, \boldsymbol{r})$, the production rate of secondary particles, and can be written schematically as:

$$Q_s(E, \boldsymbol{r}) = 4\pi \int \frac{d\sigma_{P \to s}(E, E')}{dE} \frac{\rho(\boldsymbol{r})}{\langle m \rangle} J_P(E', \boldsymbol{r}) dE' \,. \quad (2)$$

$J_P(E, \boldsymbol{r})$ is the flux of primaries at position $\boldsymbol{r}$ in the Galaxy, which is assumed to be uniform throughout (at least) the Galactic disk including the region near Earth (just outside the heliosphere). The interstellar density ρ drops off outside the disk, and diffusion occurs in a region that includes both the gaseous disk and some part of a halo. The quantity $\langle m \rangle$ is the average mass of an interstellar atom. The same $\rho(\boldsymbol{r})$ and $J_P(E, \boldsymbol{r})$

are used in the calculation of both secondary nuclei and antiprotons. The main difference is that, for secondary nuclei, only primaries with atomic numbers greater than those of the relevant secondaries are used. In addition, the spallation cross sections for production of secondary nuclei are approximately proportional to a Dirac delta function $\delta(E - E')$, so the integral over energy per nucleon collapses.

The next term is the secondary loss rate due to diffusive (with diffusion coefficient D) and convective (with convection velocity $\boldsymbol{u}$) flows out of the Galaxy. Here we are not concerned with the details of how the particles move in the Galaxy but rather with the temporal and spatial (over the Galactic disk) averaged values of the secondary flux. In this spirit we can replace the diffusive-convective term with $N_s(E)/\tau_e(E)$, where the characteristic time $\tau_e(E)$ has different interpretations in different models. In the leaky box model it is the mean escape time from the containment region. In a diffusion model it is the residence time in the gaseous disk. In both cases, the disk is assumed to be the source region for secondary cosmic rays (antiprotons as well as nuclei). In diffusion models the disk also contains the sources of the primary cosmic rays. In a diffusion picture "residence" time $\tau_e(E)$ is related to a combination of the diffusion coefficient and Galactic dimensions. It is generally believed that this escape time depends on rigidity, not energy; thus, the energy dependence of the escape time is different for secondary nuclei and antiprotons. The main point we wish to emphasize is that our results follow from the assumption that antiprotons are produced in the same regions as secondary nuclei (i.e., from collisions in the interstellar medium [ISM]), and they see the same Galactic diffusion as the secondary nuclei. This assumption holds in the "leaky box" model or "leakage lifetime approximation" and also in more general diffusion models.[1]

The third term on the right-hand side of equation (1) represents the loss due to inelastic collisions, with characteristic time τ_i. An antiproton can survive the inelastic collision, albeit with a lower final energy, so to be correct we should also include a term to account for these surviving antiprotons. However, the fact that the residence time is shorter than the interaction time ensures that these surviving antiprotons will make only a small contribution to the flux. This is especially true at high energy, since the residence time τ_e decreases with energy. We have used the cross sections given in Tan & Ng (1983) to calculate the effect of including inelastic scattering. We find that inelastically scattered antiprotons contribute less than 10% of the flux at kinetic energies $\gtrsim 2$ GeV, and the fraction decreases as the energy increases. If one considered a closed galaxy model, for which the residence time is assumed to be very much greater than the interaction time, the inelastically scattered antiprotons would become an important source of $\bar{p}$ flux (Protheroe 1981). Since we are mainly interested in the antiprotons at energies of $\gtrsim 2$ GeV with short residence times, we will ignore the inelastically scattered antiprotons.

The last term describes the energy loss or gain of secondaries as they propagate. The term $b(E)$ is the average rate of energy change for a secondary of energy E. The only significant energy losses for antiprotons and nuclei are from plasma scattering and ionization, both of which are irrelevant for antiprotons at kinetic energies $\gtrsim 1$ GeV. The $b(E)$ term can also represent possible "reacceleration" as the particle travels through the Galaxy. This reacceleration must occur on some level, but its importance is not well known. Here we will ignore reacceleration, keeping in mind that reacceleration can affect the $\bar{p}/p$ ratio (Simon, Heinbach, & Koch 1987).

With these simplifications, equation (1) reduces to

$$\frac{1}{\tau_e} N_s(E) + \frac{1}{\tau_i} N_s(E) = Q_s(E) \,. \tag{3}$$

It will be more convenient to work in terms of flux, $J_s(E) = vN_s(E)/(4\pi)$:

$$J_s(E) = \frac{v\tau_e}{1 + \tau_e/\tau_i} \frac{Q_s(E)}{4\pi} \,, \tag{4}$$

where v is the secondary particle velocity. The characteristic time τ_e depends on the energy of the propagating (secondary) cosmic-ray nucleus or antiproton. It is related to an "escape length" by

$$\lambda_e(E) = v\rho\tau_e(E) \,. \tag{5}$$

Specializing to the antiproton case, the source term is explicitly written

$$\frac{Q_{\bar{p}}(E)}{4\pi} = 2 \frac{\rho}{m_{\rm H}} \epsilon \int \frac{d\sigma_{pp\to\bar{p}}}{dE_{\bar{p}}} J_p(E_p) dE_p \,, \tag{6}$$

where $\sigma_{pp\to\bar{p}}$ is the cross section for proton-proton $\to$ antiproton + anything. The factor ϵ is needed to account for effects of nuclei in the interstellar gas and in the cosmic-ray beam, and the factor of 2 accounts for antiprotons produced by antineutron decay. This source spectrum of antiprotons is quite narrow, with most of the yield between 0.5 and 15 GeV.

2.1. *The Local Interstellar Spectrum*

From equation (6) we can see that the antiproton flux depends directly on the energy spectrum of the primary cosmic rays. Any uncertainty in the normalization and shape of the primary spectrum thus leads to a corresponding uncertainty in the calculated antiproton spectrum. To see what primary energies are most important, it is helpful to look at the response curves for produced antiprotons in Figure 1, which shows the integrand of the source term (6) normalized to the value of the total integral. The six curves correspond to the differential fraction of antiprotons at energy $E_{\rm pbar}$ produced by primary protons of kinetic energy E_p. An important kinematic effect of the high threshold energy for antiproton production is that even low-energy antiprotons require high energy for their production (Gaisser & Levy 1974). In fact, as E_p decreases below 1 GeV kinetic energy, the mean parent energy *increases*. This kinematic feature has two consequences for antiproton production: (1) there is a suppression of the intensity of antiprotons below 1 GeV, and (2) only primaries with $E \gtrsim 10$ GeV are important in the source calculation (6), and in this high-energy regime uncertainties in the parent spectrum due to solar modulation are relatively unimportant.

The spectral index of the primary proton spectrum above 10 GeV is known to a high degree of accuracy. From any given experiment, the calculated fits to rigidity spectra find spectral index errors in only the third significant digit. However, this small error is still significant for calculating the antiproton flux at energies of a few GeV. Over this range of energies, an error

[1] This issue has been discussed in a number of references. For the relation to a diffusion model see, e.g., Cesarsky & Ormes (1987) or chap. 9 in Gaisser (1990).

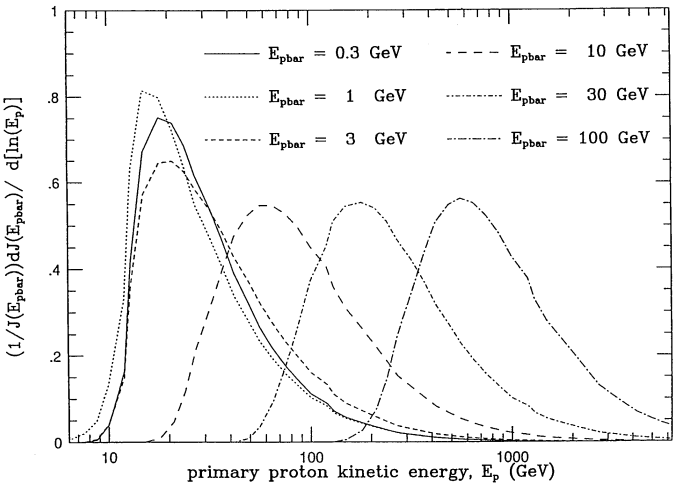

FIG. 1.—Fraction of antiprotons of energy E_{pbar} produced by primary protons of kinetic energy E_p. The threshold for antiproton production (6 GeV) is apparent. Antiprotons with energies below 1 GeV must be produced with large backward momentum in the center of the momentum frame, and hence are mostly produced by large energy primaries.

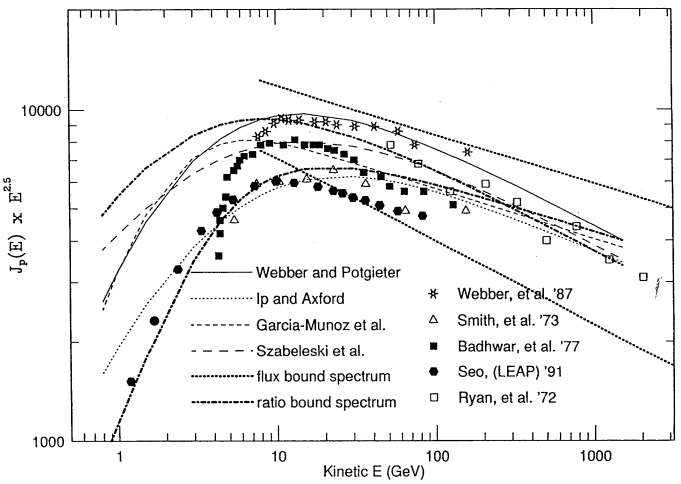

FIG. 2.—Interstellar proton spectra. The data are from the following references: Ryan, Ormes, & Balasubramanyan (1972), Smith et al. (1973), Badhwar et al. (1977), Webber, Golden, & Stephens (1987), and Seo (1991). The rough shape of the interstellar proton spectrum is generally agreed upon, but the normalization and the steepness of the rolloff below a few GeV are somewhat uncertain. Plotted are some examples of fits (Szabeleski, Wdowczyk, & Wolfendale 1980; Webber & Potgieter 1989; Garcia-Munoz, Mason, & Simpson 1975; Ip & Axford 1985), as well as some spectra we have designed to give upper and lower bounds to the $\bar{p}$ flux and the $\bar{p}/p$ ratio.

of ± 0.05 in the spectral index leads to a 20% spread in the antiproton flux at 5–15 GeV energies.

The range of high-energy proton spectra is shown in Figure 2. The heavy dotted lines indicate extreme ranges of spectra that we use to estimate the uncertainty in the calculated interstellar antiproton intensity from this source. The motivation for these forms is discussed in detail in an appendix. Basically, there are two uncertainties. the spectral exponent and the normalization. Averaging over all experiments in Figure 2, we find that the data can be well fitted with a spectral exponent in the narrow range of 2.65–2.75. However, the absolute fluxes reported vary by $\sim \pm 25\%$. Given the enormous difficulty of determining absolute fluxes at the top of the atmosphere, this normalization difference may well be due to systematic experimental errors. To quantify the spectrum errors, we take the hardest $\gamma = 2.65$ spectrum with the highest measured (Webber, Golden, & Stephens 1987) fluxes (upper-bound spectrum) and the softest $\gamma = 2.75$ spectrum with the lowest measured (Seo 1991) fluxes (lower-bound spectrum).

2.2. *Path Lengths in the Galaxy*

The escape length that governs propagation of secondary cosmic rays (antiprotons as well as nuclei) is determined by fitting the observed ratios of secondary to primary nuclei (e.g., *B/C*). A good fit to the high-energy secondary abundances is obtained by describing the path length as a power law in rigidity, just as would be expected in diffusion models (Ginzburg & Ptuskin 1976). As the rigidity is lowered below ≈ 4 GV, the path length decreases, which can be modeled as a power law in the particle velocity. This can happen in some Galactic propagation models, since the escape mechanism becomes convection instead of diffusion at these rigidities. Since the measurements of the *HEAO 3* satellite, the values of the path length can be calculated with some precision. A large number of groups have independently calculated fits to the path length, and a sampling of post–*HEAO* fits is plotted in Figure 3. Recently, the French-Danish collaboration which operated the *HEAO 3* C-2 cosmic-ray heavy nuclei experiment have reanalyzed their data (Engelmann et al. 1990) and, for reasons we will discuss, found a somewhat larger path length, which is also displayed in Figure 3.

The path length depends on rigidity. Since the relation between rigidity and energy per nucleon differs significantly for secondary nuclei and for particles with $Z = A$ (i.e., protons and antiprotons), some care is needed in translating from the escape lengths determined from secondary nuclei to those appropriate for antiprotons. This is especially important at low energy.

A parameterization used by Ormes & Protheroe (1983) is

$$\lambda_e = \Lambda \left[\frac{1}{1 + (R_0/R)^2} \right]^{n/2} R^{-\delta}, \qquad (7)$$

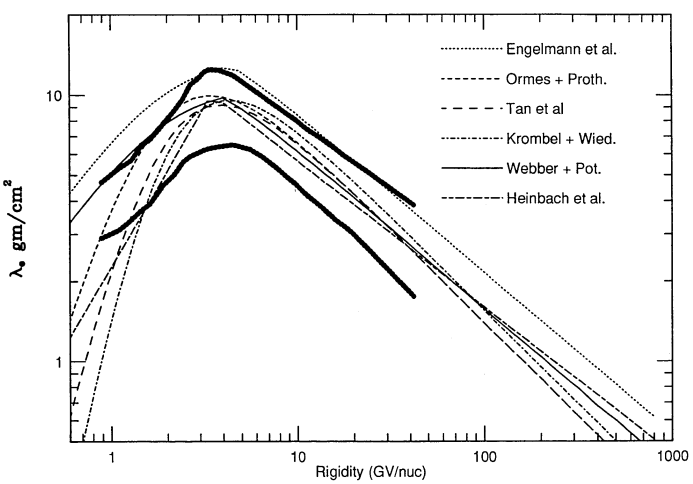

FIG. 3.—Different fits to the path length (Engelmann et al. 1990; Webber & Potgieter 1989; Ormes & Protheroe 1983; Tan et al. 1987; Krombel & Wiedenbeck 1987; Heinbach & Simon 1990). The heavy dotted lines are the estimated maximal errors to the path-length fit given in Garcia-Munoz et al. (1987). Path lengths agree roughly for energies above 3 GV; however, the fits show a large spread below this energy.

where R is the rigidity (in GV) of the particle; Λ, n, and δ are constants fitted to the data; and R_0, also fitted, is the rigidity above which diffusion becomes more important than convection. Ormes & Protheroe used $R_0 = 1.88$ GV, which, for nuclei with $A/Z = 2$, reduces the form of the path length to

$$\lambda_e = \Lambda \beta^n R^{-\delta} , \tag{8}$$

where βc is the velocity. Ormes & Protheroe (1983) found a good fit with $n \sim 3$, although typically $n = 1$ is now found to be in better agreement (Cesarsky 1987). In order to find the appropriate escape lengths for antiprotons, we have replaced β by $\beta/(4 - 3\beta^2)^{1/2}$, as would be appropriate in the parameterization of Ormes & Protheroe for $A/Z = 1$, and plotted the results in Figure 3. It is not clear that this is the proper way to parameterize the low-energy path length for both particles and nuclei. In fact, Webber & Potgieter (1989) do not make this substitution. However, this uncertainty only affects very low energy particles. For instance, the difference between making and not making our substitution for β leads to a difference of less than 10% in the path length for kinetic energies above 3 GeV.

All of the path lengths in Figure 3 agree roughly in the rigidity range 2 GV $\leq R \leq$ 50 GV, although the agreement is worst below 2 GV, possibly owing to large uncertainties from solar modulation effects. The main uncertainties in these path-length calculations are due to three sources of error: (1) there are uncertainties in the measured secondary-to-primary ratios, (2) the calculations require nuclear cross sections, some of which are not measured and have to be estimated, and (3) at low rigidities there are small uncertainties due to the effects of solar modulation. A comprehensive set of the data on elemental abundances has been compiled by Garcia-Munoz et al. (1987), who have used these data to evaluate path lengths and the path-length distribution function. They find an average path length which is in good agreement with those in Figure 3, at least for rigidities $\gtrsim 2$ GV, where solar modulation effects are not expected to be too important. They also found evidence for a depletion of short path lengths, but this was unimportant for cosmic rays of $\gtrsim 1$ GV nucleon^{-1}, so we will not include this effect.

More important, Garcia-Munoz et al. have estimated the size of the maximum systematic error in average path lengths, represented in Figure 3 by the heavy dotted lines. The maximum possible error is roughly a range of $\pm 35\%$ from their best-fit mean value. With the exception of the Engelmann et al. (1990) result, the path lengths are well within the Garcia-Munoz et al. error estimates above 4 GV, with the Webber & Potgieter (1989) value closest to the Garcia-Munoz et al. mean. Below 2 GV the agreement is not as good. The Webber & Potgieter path length is close to the estimated upper limit of Garcia-Munoz et al. and that of Heinbach & Simon (1990) is close to the lower bound of Garcia-Munoz et al. This is the regime where solar modulation effects are important, and some of the extra discrepancy may be due to solar modulation uncertainties. Thus below 4 GV, we will allow for a larger error than do Garcia-Munoz et al. in our estimate for total possible error, partly to cover solar modulation uncertainties and also to cover uncertainties in the low-energy path-length parameterization.

The new path length of Engelmann et al. (1990) differs from the results of older calculations, including previous results from that same group, in several important ways. First, they have used new data on helium cross sections (see Ferrando et al. 1988) to determine the production of nuclear secondaries. They also have reanalyzed the data from the *HEAO 3* experiment with new and more accurate estimates of instrumental corrections, with the result that the measured boron/carbon ratios have changed slightly. Both of these effects should be accounted for in the Garcia-Munoz et al. error estimate, and, indeed, these two effects alone will not cause the path length to be larger than the maximum estimate in Figure 3. There are two more pieces of information included in the Engelmann calculation which push the path length to a value just outside the error range. The major effect is that they have included energy losses from propagation in the ionized component of the interstellar material (Soutoul & Ferrando 1989), which is quite important for nuclei (because of the Z^2 dependence) at several GeV nucleon^{-1} energy but can be neglected for antiprotons with greater than GeV energy. To compensate for these energy losses, the path length at higher energies have to be slightly increased. Another minor effect is that Engelmann et al. (1990) have used a slightly higher helium concentration (10% versus 7% of Garcia-Munoz et al. 1987), which results in a smaller number of interstellar targets per gram of interstellar material, implying that a longer path length is needed. We agree with the approach of the Engelmann et al. calculation, i.e., that they are using the right ingredients for the best possible calculation. Thus we ought to use their path length as a baseline for our calculation and consider an error range about their calculated value. The errors in cosmic-ray flux measurements from *HEAO* and uncertainties from unknown nuclear cross sections have been reduced, so presumably the error range of Garcia-Munoz et al. is too generous. However, to be overly conservative, for our upper limit on the size of the path length we will use the full $+35\%$ error range applied to the Engelmann et al. path length (i.e., 1.35 times the Engelmann et al. value of Λ). For the lower limit we will use the -35% error applied to the Tan et al. (1987) path length. This will allow for a very large range of path lengths to cover any other uncertainties.

As Webber has emphasized, many of the previous calculations of the $\bar{p}/p$ ratio were done at a time when estimates of the path length were somewhat smaller than the path lengths in Figure 3, at least in the energy range covered by the Golden et al. (1984) measurements (4–13 GeV). For example, in 1981, the best current value of the path length (Protheroe 1981) was 7 $(R/4\ \mathrm{GV})^{-0.4}$ g cm^{-2}, which decreases to 4.8 g cm^{-2} at 10 GV. This is nearly a factor of 2 below the most recent estimates of escape path length. Thus we conclude that it is important to use modern values of the path length (as pointed out by Webber & Potgieter 1989) in calculations of the antiproton flux. Further discussion of the results will be postponed until after a derivation of the nuclear factors in the next section.

2.3. *Nuclear Factors*

In this section we consider the effect of nuclei in the cosmic radiation and the interstellar medium. The flux of antiprotons at a given energy will have the value where $\bar{p}$ production is balanced by $\bar{p}$ escape (eq. [4]):

$$J_{\bar{p}}(E_{\bar{p}}) = \frac{2v\tau_e}{1 + \tau_e/\tau_i} \sum_i^{\mathrm{CR}} \sum_T^{\mathrm{ISM}} \frac{\rho_T}{m_T} \int \frac{d\sigma_{iT\to\bar{p}}}{dE_{\bar{p}}} J_i(E_i) dE_i . \tag{9}$$

Here J_i is the flux incident particles of type i, τ_e is the residence time in the Galactic disk, the leftmost sum is over the types of

(incident) nuclei present in the cosmic-ray flux, and the rightmost sum is over the nuclei (targets) in the ISM; m_T and ρ_T are the mass density of nuclei in the ISM, and $\sigma_{iT\to p}$ is the cross section for production of antiprotons resulting from the collision of nuclei i and T. The factor of 2 in front of the integral accounts for the production of antineutrons, which quickly decay into antiprotons. We would like to rewrite this in terms of an incident spectrum of primary protons colliding with hydrogen targets and treat the presence of heavier nuclei in cosmic rays and the ISM as a multiplicative "enhancement" factor ϵ.

First we rewrite this equation in terms of parameters more convenient for the calculation of this factor ϵ. We scale ρ_T and $J_i(E_i)$ in terms of abundances relative to hydrogen:

$$\frac{\rho_T}{m_T} = \frac{\rho_T}{\rho_H}\frac{m_H}{m_T}\frac{\rho_H}{m_H} = \left(\frac{n_T}{n_H}\right)\Bigg|_{ISM}\frac{\rho_H}{m_H}. \tag{10}$$

The next factor is the incident spectra. The ratios of fluxes of heavier nuclei to protons in the cosmic rays is roughly constant (Simpson 1983) above a few GeV nucleon^{-1}, and this is the range of importance for $\bar{p}$ production. Thus the incident flux of all cosmic-ray species can be written approximately as proportional to the incident proton flux at a fixed energy per nucleon:

$$J_i(E_i) = \left[\frac{n_i(E_i)}{n_p(E_i)}\right]\Bigg|_{CR} J_p(E_p), \tag{11}$$

where the subscript CR indicates these abundances are the abundances in the cosmic rays. Our differential $\bar{p}$ spectrum equation now apears as

$$J_{\bar{p}}(E_p) = \frac{2v\tau_e\rho_H}{m_H(1+\tau_e/\tau_i)}\sum_i^{CR}\sum_T^{ISM}\left(\frac{n_i}{n_p}\right)\Bigg|_{CR}\left(\frac{n_T}{n_H}\right)\Bigg|_{ISM} \times \int \frac{d\sigma_{iT\to\bar{p}}}{dE_{\bar{p}}} J_p(E_p)dE_p. \tag{12}$$

We evaluate any dependence of the cross section on the incident energy per nucleon at the value of the incident proton energy in equation (12). The ratio of cosmic-ray abundances therefore must be evaluated at the same energy per nucleon.

In order to compute the flux of antiprotons produced, we need the cross section for $\bar{p}$ production from nuclear collisions. While the cross section for $pp\to\bar{p}$ has been fairly well measured, the cross sections for heavier nuclear are not. A theoretical model of the scaling of the production cross section exists called the "wounded nucleon" model (Bialas, Bleszynski, & Czyz 1976), which seems to describe nuclear collisions quite well. It is successful at predicting pion and kaon multiplicities in proton-nucleus collisions (Brick et al. 1989) at high energies (200 GeV protons on nuclear targets), and, more important for the cosmic rays, in helium-helium collisions at energies $(s)^{1/2} = 31.5$ and 44 GeV nucleon^{-1} in experiments at the CERN ISR (Akesson et al. 1982; Faessler 1984). We here assume that the wounded nucleon model also correctly relates the $\bar{p}$ multiplicity in nuclear collisions to that in pp collisions, although this remains to be experimentally tested. The basic idea is that in a nuclear collision, an incoming nucleon can strike more than one nucleon on its way through the nucleus, and that each struck nucleon contributes a multiplicity equal to half that of an independent nucleon-nucleon collision. The number of wounded nucleons is found by averaging the nuclear shapes over impact parameters and dividing by a proton diameter. The multiplicitly of produced particles in a collision between a nucleus with A nucleons (nucleus A) and a nucleus with B nucleons (nucleus B) is given by (Bialas et al. 1976)

$$n_{AB} = \frac{1}{2}\left(\frac{A\sigma_{pB,inel}}{\sigma_{AB,inel}} + \frac{B\sigma_{pA,inel}}{\sigma_{AB,inel}}\right)n_{pp} \equiv \frac{1}{2}w_{AB}n_{pp}, \tag{13}$$

where $\sigma_{AB,inel}(\sigma_{pA,inel})$ is the total inelastic cross section for a collision between nucleus A and nucleus B (between a proton and nucleus A) and n_{pp} is the mean multiplicity of a pp collision. The terms inside the parenthesis are respectively the number of wounded nucleons in nucleus A and nucleus B, and w_{AB} is the total number of wounded nucleons.

It is also necessary to account for the fact that the nuclear cross section is larger than a proton cross section. Thus we write

$$\sigma_{iT\to\bar{p}} \simeq \frac{1}{2}w_{iT}\frac{\sigma_{iT,inel}}{\sigma_{pp,inel}}\sigma_{pp\to\bar{p}} = \frac{1}{2}(A_i\sigma_{pT,inel} + A_T\sigma_{pi,inel})\frac{\sigma_{pp\to\bar{p}}}{\sigma_{pp,inel}}, \tag{14}$$

where A_i, A_T are the atomic numbers of the incident and target nucleons. The crucial assumption here is that the momentum distribution of produced antiprotons has the same shape in nuclear collisions as in pp collisions. The inelastic p-nucleus cross sections are measured, and analytic fits can be found for them (Letaw, Silberberg, & Tsao 1983). Hereafter we will drop the "inel" subscript from the cross sections and note that all cross sections which appear will be the inelastic cross sections.

Using the scaling for the cross sections, then, we have

$$J_{\bar{p}}(E_{\bar{p}}) = \frac{v\tau_e\rho_H}{\lambda_p\sigma_{pp}(1+\tau_e/\tau_i)}\sum_i^{CR}\sum_T^{ISM}\left(\frac{n_i}{n_p}\right)\Bigg|_{CR}\left(\frac{n_T}{n_H}\right)\Bigg|_{ISM} \times w_{iT}\frac{\sigma_{iT}}{\sigma_{pp}}\int\frac{d\sigma_{pp\to\bar{p}}}{dE_{\bar{p}}}J_p(E_p)dE_p, \tag{15}$$

where $\lambda_p = m_H/\sigma_{pp}$ is a proton interaction length in hydrogen.

In order to get a numerical prediction for the $\bar{p}$ flux, we need numerical values of τ_e and the average ρ_H seen by cosmic rays. Information about these parameters is contained in the "path length" described in the previous section. One then usually makes some assumptions about the type of material through which the cosmic rays must pass. For example, Webber & Potgieter (1989) use a path length determined by assuming that the ISM is 100% hydrogen. Thus their escape length is $\lambda_e^H = v\rho_H\tau_e$. Garcia-Munoz et al. (1987) assume that the interstellar medium is a mixture of 93% hydrogen and 7% helium; thus

$$\lambda_e^M = v(\rho_H^M + \rho_{He}^M)\tau_e = 1.30v\rho_H^M\tau_e. \tag{16}$$

We will calculate the $\bar{p}$ enhancement factor due to heavier nuclei in two scenarios: that of a pure hydrogen ISM and a hydrogen-helium mixture. We will ignore all elements heavier than helium in the ISM. This is consistent, even though we include these heavier nuclei in the cosmic-ray flux, because the escape path lengths are derived using these assumptions. Including the heavier elements in our calculation would be correct only if we had escape times derived with the same ISM composition. We expect that including the heavier elements in the ISM would change $\bar{p}$ production but would also alter the

required escape time in such a way that the two factors would cancel somewhat.

2.3.1. *Pure Hydrogen Interstellar Medium*

The formula for the equilibrium spectrum of antiprotons simplifies in the case of a pure hydrogen ISM to

$$J_{\bar{p}}(E_{\bar{p}}) = \frac{2\lambda_e^{\rm H}}{(\lambda_p + \lambda_e^{\rm H})\sigma_{pp}} \epsilon^{\rm H} \int \frac{d\sigma_{pp\to\bar{p}}}{dE_{\bar{p}}} J_p(dE_p)dE_p \,, \qquad (17)$$

where we have defined the escape path length in hydrogen as

$$\lambda_e^{\rm H} = v\tau_e \rho_{\rm H} \,,$$

and $\epsilon^{\rm H}$ is the nuclear enhancement factor in a hydrogen ISM:

$$\epsilon^{\rm H} = \sum_i^{\rm CR} \left(\frac{n_i}{n_p}\right)\Big|_{\rm CR} \frac{1}{2} w_{ip} \frac{\sigma_{ip}}{\sigma_{pp}} \equiv \sum_i^{\rm CR} \left(\frac{n_i}{n_p}\right)\Big|_{\rm CR} m_{ip} \,. \qquad (18)$$

This sum is evaluated term by term in Table 1, with the result that

$$\epsilon^{\rm H} = 1.20 \,. \qquad (19)$$

Thus the resulting $\bar{p}$ flux will be 20% larger than if the cosmic rays were pure hydrogen. The cosmic-ray abundances in Table 1 were taken from the review article by Simpson (1983), with the exception of helium, which was taken from Webber et al. (1987). We note that it is important to use high-energy abundances, since the threshold for $\bar{p}$ production is about 6 GeV nucleon.$^{-1}$

2.3.2. *Mixed Interstellar Media*

Here we consider an ISM composed of 93% H and 7% He. Again we write the $\bar{p}$ flux as

$$J_{\bar{p}}(E_{\bar{p}}) = \frac{2\lambda_e^M}{(\lambda_p + \lambda_e^M)\sigma_{pp}} \epsilon^M \int \frac{d\sigma_{pp\to\bar{p}}}{dE_{\bar{p}}} J_p(E_p)dE_p \,, \qquad (20)$$

where $\lambda_e^M = 1.30 v\tau_e^M \rho_{\rm H}^M$ and

$$\epsilon^M = \frac{1}{1.30} \sum_i^{\rm CR} \left(\frac{n_i}{n_p}\right)\Big|_{\rm CR} \frac{1}{2}\left[w_{ip}\frac{\sigma_{ip}}{\sigma_{pp}} + \frac{\sigma_{i\alpha}}{\sigma_{pp}}\left(\frac{n_\alpha}{n_{\rm H}}\right)_{\rm ISM} w_{i\alpha}\right]. \qquad (21)$$

Here τ_e^M is the escape time determined by allowing the cosmic-ray nuclei to propagate through a mixed ISM. The 1.30 in equation (21) is from the presence of helium (see eq. [16]). Equation (21) can also be written in a simpler way:

$$\epsilon^M = \frac{1}{1.30}\left(\epsilon^{\rm H} + \frac{0.07}{0.93}\epsilon^{\rm He}\right), \qquad (22)$$

where we have used the definition of $\epsilon^{\rm H}$ from the previous section and now similarly define

$$\epsilon^{\rm He} = \sum_i^{\rm CR} \left(\frac{n_i}{n_p}\right)\Big|_{\rm CR} \frac{1}{2} w_{i\alpha} \frac{\sigma_{i\alpha}}{\sigma_{pp}} = \sum_i^{\rm CR} \left(\frac{n_i}{n_p}\right)\Big|_{\rm CR} m_{i\alpha} \,. \qquad (23)$$

TABLE 1

NUCLEAR CONTRIBUTIONS TO $\epsilon_{\rm H}$ AND $\epsilon_{\rm He}$

Nucleus	A_i	v_i[a]	$n_i/n_{\rm H}\vert_{\rm CR}$[b]	m_{ip}[c]	ϵ_H[d]	$m_{i\alpha}$[c]	$\epsilon_{\rm He}$[d]
H	1	1	1	1	1	3.57	3.57
He	4	1.27	0.042	3.57	0.150	12.6	0.53
Li	7	1.28	2.3×10^{-4}	6.1	0.0014	22	0.005
Be	9	1.39	1.2×10^{-4}	7.7	0.0009	22	0.004
B	11	1.48	3.6×10^{-4}	9.0	0.0032	32	0.011
C	12	1.52	1.2×10^{-3}	9.9	0.0119	36	0.043
N	14	1.58	3.2×10^{-4}	11.4	0.0036	40	0.013
O	16	1.64	1.0×10^{-3}	12.9	0.0129	47	0.047
F	19	1.73	2.3×10^{-5}	15	0.0003	52	0.001
Ne	20	1.76	1.7×10^{-4}	16	0.0027	55	0.009
Na	23	1.82	3.6×10^{-5}	18	0.0006	62	0.002
Mg	24	1.86	4.2×10^{-5}	19	0.0008	64	0.003
Al	27	1.92	3.8×10^{-5}	20	0.0008	71	0.003
Si	28	1.94	1.7×10^{-4}	21	0.0036	73	0.012
P	31	2.00	1.0×10^{-5}	23	0.0002	80	0.001
S	32	2.02	3.3×10^{-5}	24	0.0008	82	0.003
Cl	35	2.08	8.0×10^{-6}	26	0.0002	90	0.001
Ar	40	2.16	1.4×10^{-5}	29	0.0004	100	0.001
K	39	2.14	1.1×10^{-5}	29	0.0003	98	0.001
Ca	40	2.16	2.2×10^{-5}	29	0.0006	100	0.002
Sc	45	2.24	5.6×10^{-6}	32	0.0002	111	0.001
Ti	48	2.28	1.5×10^{-5}	34	0.0005	118	0.002
V	51	2.32	7.8×10^{-6}	36	0.0003	124	0.001
Cr	52	2.34	1.5×10^{-5}	37	0.0006	126	0.002
Mn	55	2.38	1.1×10^{-5}	39	0.0004	133	0.002
Fe	56	2.39	1.1×10^{-4}	40	0.0044	135	0.015

[a] The cross sections used in the calculation of the number of wounded nucleons were taken from Letaw, Silberberg, & Tsao 1983, except for the helium cross sections, which were found in Faessler's 1984 review of CERN ISR experiments.

[b] The helium abundance at greater than a few GEV energies is derived by Webber Golden, & Stephens 1987, which (within errors) agrees with the result of Seo 1991. For the heavier elements we use the abundances for energies of 1–2 GeV from Simpson's 1983 review article.

[c] Antiproton multiplicities are defined as $m_{ip} \equiv \frac{1}{2}\sigma_{pi} w_{pi}/\sigma_{pp}$ and $m_{i\alpha} \equiv \frac{1}{2}\sigma_{\alpha i} w_{\alpha i}/\sigma_{pp}$.

[d] Totals: $\epsilon_{\rm H} = 1.20$; $\epsilon_{\rm He} = 4.28$.

We have evaluated ϵ^{He} in Table 1 and found it to have the value of

$$\epsilon^{He} = 4.28 . \quad (24)$$

Thus the total nuclear factor for this mixed medium is

$$\epsilon^{M} = \frac{1.20 + (0.075)(4.28)}{1.30} = \frac{1.52}{1.30} = 1.17 . \quad (25)$$

This is 3% lower than that of a pure hydrogen ISM, but we would expect that this difference will be compensated by a larger value of λ^M compared with λ^H. To see this effect for antiprotons, just note that for the same ISM mass density we count the helium as weighing the same as four protons. However, the yield (in secondary production) of those helium atoms is somewhat less than the yield of four protons, i.e.,

$$\tfrac{1}{2} w_{p\alpha} \sigma_{p\alpha} = 3.57 \sigma_{pp} ,$$

so that the helium counts as only 3.57 protons in terms of secondary yield. Thus, to give the same $\bar{p}$ yield, the cosmic rays would need to stay confined in the Galaxy for a 3% longer time.

$$\frac{\tau_e^M}{\tau_e} = \frac{0.93 + 0.07(4)}{0.93 + 0.07(3.57)} = 1.03 .$$

A similar lengthening of path lengths has been seen for secondary nuclei as well (Ferrando et al. 1988). This difference is small compared with other uncertainties in the calculation, and we can ignore for now the ISM composition assumed when path lengths are determined.

We estimate the error in our value of ϵ to be no more than about $\lesssim 10\%$. The accuracy of our calculation depends on the elemental abundances, the p-nucleus cross sections, and the precision of the wounded nucleon model. For helium, the major contributor to ϵ, all of these ingredients are known very well. Thus, even if we make an error of 50% in our helium contribution, we change ϵ by $(0.5 \times 0.15)/1.20 \times 100\% = 6\%$. If we were to make an error of a factor of 2 in the heavier element contribution, this would change ϵ by less than 5%. Thus we do not expect that our value of ϵ will change by more than 10% with new measurements.

We make another conceptual error by assuming that nuclear cross sections for antiproton production scale as a purely multiplicative factor independent of energy relative to the pp cross section. In fact, we expect the energy distribution of heavy nuclei produced antiprotons to be somewhat different from that of a pp collision. More precisely, we know that, in the center of momentum/nucleon frame, the rapidity distribution of produced antiprotons is asymmetric, whereas the pp collision distribution is symmetric. This means we should expect that cosmic-ray protons colliding with an ISM nucleus will produce antiprotons with a lower average energy than a proton-proton collision with the same energy per nucleon. Similarly, a cosmic-ray nucleus colliding with an ISM proton will produce antiprotons with a slightly higher average energy. One expects this fact to have little effect on the $\bar{p}$ energy spectrum because the average $\bar{p}$ momentum is shifted only slightly, and heavy nuclei make up only a small fraction of matter. We have explicitly evaluated this effect for a case where we ignored elements heavier than helium in the cosmic rays and the ISM. Using a Monte Carlo program, we calculated the energy distributions of antiprotons in a proton-helium collision. We found that the average momentum of the antiprotons changed by +5% (−5%) in the laboratory or Galactic frame of reference, when the helium atom was the projectile (target). The result of including this effect was that the $\bar{p}/p$ ratio changed by ~1%. Thus we feel we can simply scale the proton-proton collision cross section without making appreciable errors.

2.3.3. *Comparison with Other Calculations*

Our value of 1.20 for ϵ is not too far from earlier determinations; for example, Szabeleski, Wdowczyk, & Wolfendale (1980) (who considered only helium nucleus contributions) found 1.25, and Orth & Buffington (1976) found 1.34. The Orth & Buffington value differs from ours mainly in the calculation of the multiplicity enhancement factor. Although the procedures for calculating multiplicities are somewhat different, the basic disagreement is as follows. In our model, each "wounded" nucleon is responsible for one-half of the yield in a pp collision (thus in a pp collision we have half the yield from the target and half from the projectile). Orth & Buffington assume that each participating nucleon yields four-fifths of a pp collision, so their multiplicities are considerably larger than ours. These multiplicities were used by Webber & Potgieter (1989), along with cosmic-ray nuclear abundances which are somewhat larger than the ones used here, to get a nuclear enhancement factor of $\epsilon = 1.59$.

2.4. *Results: Interstellar Predictions*

We now combine the most extreme values of parameters, using estimates of maximum possible error to show the range of $\bar{p}$ fluxes and $\bar{p}/p$ ratios expected for antiprotons produced purely as secondary particles. We summarize these results in Figure 4 where we plot a band of predicted values which is allowable given our estimates of the error, and the geometric mean value in that band. The errors are more than a factor of 2 from the geometric mean value. For the high extreme bound of our error we have used the high bounding interstellar spectrum, the Engelmann et al. (1990) path length multiplied by

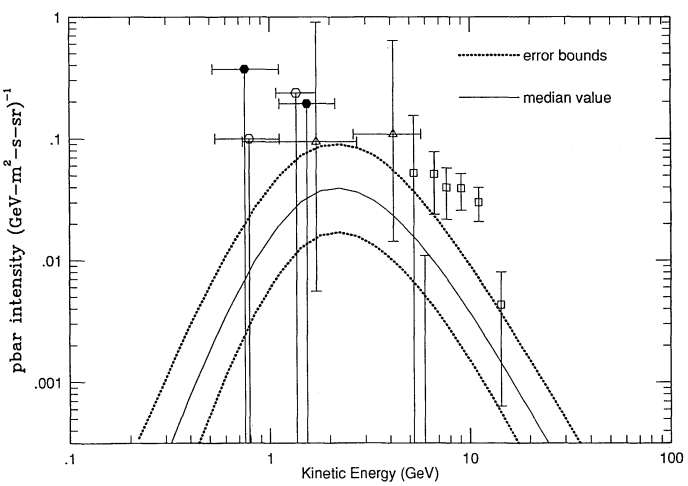

FIG. 4.—Interstellar $\bar{p}$ flux and the maximum possible error estimated from combining uncertainties in the ingredients of the antiproton calculation as described in the text. We have drawn a curve corresponding to the geometric mean value between the minimum and maximum errors. No solar modulation is done. We have plotted the corresponding interstellar $\bar{p}$ flux upper limits for the PBAR (*filled hexagons*; Salamon et al. 1990) and LEAP experiments (*open hexagons*; Stochai 1990; Streitmatter et al. 1989) and measured flux values from Bogomolov et al. (1987 [*triangles*]) and Golden et al. (1984 [*squares*]), as given by Perko (1992), who demodulated the antiproton and proton fluxes independently.

1.35 (to add the 35% maximum error estimate of Garcia-Munoz et al.). For the lower bound, we take the lower proton bounding spectrum, and use the path length of Tan et al. (1987) multiplied by 0.65 (again for the maximum error estimate). To each of these bounds we then have added an additional 10% to account for uncertainties in the value of the antiproton production cross section[2] at energies 10–100 GeV. This gives us a wide range of error for the $\bar{p}$ flux. We have not included errors in the nuclear factor, which we expect to be $\lesssim 10\%$.

3. COMPARISON WITH DATA

In order to compare our interstellar values with data at 1 AU, one must include the effects of solar modulation, which can be quite different for particles of opposite charge signs. For example, recent studies (Tuska 1990) have shown that the ratio of the proton to electron fluxes can vary by as much as a factor of 2 at an energy as high as 6 GeV. One way to handle this effect is to calculate the different modulations empirically by using a separate force field solution for each charge sign (Perko 1992). One fits solar modulation parameters for protons and electrons at the epoch of interest, and then modulates the p and $\bar{p}$ fluxes accordingly. By assuming the Ip & Axford (1985) electron and proton interstellar spectra (with a normalization much closer to that of Webber & Potgieter 1989), Perko (1992) has found modulation parameters appropriate for the time of each of the $\bar{p}/p$ ratio measurements. Then, by demodulating each measurement, he arrives at the corresponding $\bar{p}$ fluxes in interstellar space. These data are plotted in Figure 4. One can see that the $\bar{p}$ fluxes are consistent with the error range of our secondary $\bar{p}$ predictions, except for some of the Golden et al. measurements, which are well above the maximum predicted error, despite our generous allowances for errors in our parameters.

We can make another test of our predictions. Perko (1992) has also given modulation parameters for the force field approximation that can be used to modulate the calculated interstellar antiproton spectrum to 1 AU for comparison directly with measured $\bar{p}/p$ ratios. This is done in Figure 5 for the epoch of the Golden et al. measurements. To find the error range in this figure, we use primary p bounding spectra which are designed to maximize errors in the $\bar{p}/p$ ratio (as seen in Fig. 2). (The details of how these bounding spectra are determined can be found in the Appendix.) Once again we see that some of the Golden et al. measurements are higher than the extreme upper limit of our predictions. We must caution, however, that the modulation parameters depend on assumed interstellar proton and electron spectra, hence the conclusions of this treatment are somewhat model-dependent.

4. DISCUSSION AND CONCLUSIONS

After our examination of the factors in the $\bar{p}/p$ calculation, we find that, as Webber (1987) had suggested, our updated calculation agrees with data somewhat better than older calculations. For example, our mean ratio is up to a factor of 2 larger than that of Protheroe (1981) in the critical 4–10 GeV energy region. However, the agreement between theory and observation is still not totally satisfactory. The geometric mean value of our $\bar{p}/p$ ratio in Figure 5 is near the 3 σ limit of the combined 4–13 GeV Golden et al. value. However, data binned in smaller energy intervals within this range give a picture which does not seem so conclusive.

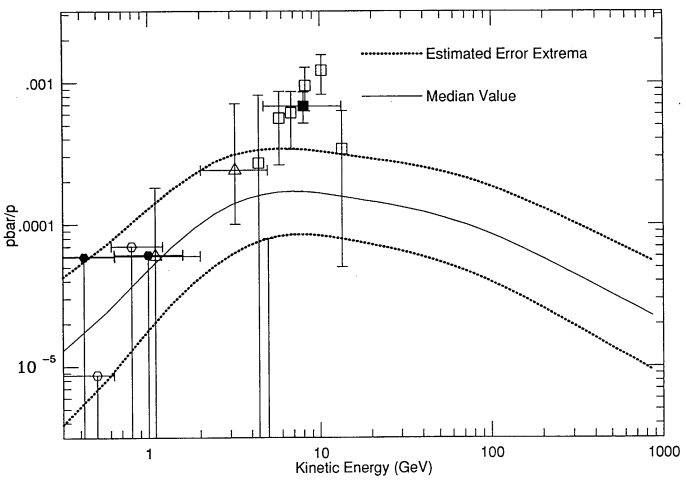

FIG. 5.—The $\bar{p}/p$ ratio modulated to its 1 AU value during the epoch of the Golden et al. (1984) data, here represented by the squares. The filled square is their combined flux value over the range of their energies. Note that the mean curve is $\sim 3.5\ \sigma$ from the combined Golden et al. measurement, while the maximum error curve is $\sim 2.5\ \sigma$ away. To get the error curves we have repeated the calculation for Fig. 4, except that we have used different bounds on the primary spectral shape as described in the Appendix. We have included other data for completeness, although the amount of solar modulation is incorrect for a proper comparison of these other data with our curve (Bogomolov et al. 1987 [*triangles*]; PBAR [Salamon et al. 1990; *filled hexagons*]; and LEAP [Stochai 1990; *open hexagons*]).

The trend of increasing $\bar{p}/p$ ratio with energy, apparent in the individual Golden et al. (1984) points, is somewhat better fitted with a model which includes distributed reacceleration (Golden et al. 1984; Simon et al. 1987). There is a great deal of recent work on reacceleration or distributed acceleration of cosmic rays, which is summarized in Cesarsky's (1987) rapporteur talk at Moscow. Although it is apparently not possible to account for all cosmic-ray acceleration as distributed acceleration simultaneous with propagation, some (weak) reacceleration is possible. The effect of weak acceleration is to boost the lower energy antiprotons to higher energy, which depletes the flux below about 4 GeV, and increases the flux (with these reaccelerated antiprotons) above this energy. However, this model will give a worse fit to the Bogomolov et al. (1987) measurement at lower energies. Also, if reacceleration were important, one would expect the highest energy Golden et al. (1984) datum to disagree most strongly with the pure secondary $\bar{p}$ flux, yet this point is consistent with purely secondary antiptrotons. For these reasons we do not feel there is enough evidence to conclude that reacceleration is required to explain the $\bar{p}$ data.

In summary, we have examined the calculation of secondary antiprotons in the cosmic radiation to look for sources of error. We find a band of possible systematic error which brackets our best-guess $\bar{p}$ fluxes and $\bar{p}/p$ ratio with a range of a factor of 2.4 about the central value. Contained in that factor is a 70% uncertainty in the magnitude of the average path length of cosmic rays in the galaxy. Another 20% is due to uncertainties in the shape and normalization of the interstellar proton spectrum.

The effect of heavy nuclei on the production yield of secondary antiprotons has been evaluated in terms of the "wounded

[2] See, for example, Fig. 9 in the review by Stephens & Golden (1987). We have determined that the uncertainty in the cross section represented by the high- and low-valued cross section fits given there yields an uncertainty of $\pm 10\%$ in the $\bar{p}/p$ ratio.

nucleon model," which is quite successful at predicting meson yields and is accurate to about 10% in proton-nucleus collisions. One would have more confidence in the model if it had been experimentally tested directly for antiproton production, but these observations are difficult to make. We have not included any estimated error for the "wounded nucleon model" in our error bands.

Other uncertainties exist, e.g., uncertainties in the parameterization of the $\bar{p}$ production cross section and asymmetries in the rapidity distribution of produced secondaries, but these errors are less than 10%. Thus we do not expect that any other effects could widen our error bounds in the secondary antiproton prediction (using the "leakage lifetime approximation"). We feel that we have been overly conservative in allowing very large errors in our upper and lower bounds on the antiproton flux prediction, and our result is still in conflict with the Golden et al. measurements. The average of the Golden et al. result in the 5–13 GeV range is still 2.2 σ above the upper bound of our prediction. We conclude that it is unlikely that the antiproton flux implied by the Golden et al. (1984) result could be explained as being due purely to secondary antiprotons

We wish to thank J. Engel, J. Perko, R. J. Protheroe, and A. Soutoul for useful discussions in the preparation of this work. We thank the referee for useful comments and providing us with the Engelmann et al. (1990) reference. This research is supported in part by NASA under NAGW-1644.

APPENDIX

THE INTERSTELLAR SPECTRA AND THE $\bar{p}/p$ RATIO TEST

In § 2.1 we consider bounds on the absolute flux of interstellar primary protons which are useful for defining uncertainties in the prediction of absolute $\bar{p}$ fluxes. However, the observed quantity is the $\bar{p}/p$ ratio. This quantity is good because it divides out the overall proton flux normalization, for which there is a large uncertainty. It is also a better number observationally, because systematic errors introduced by the detectors cancel. Unfortunately, we will introduce new uncertainties. In order to get $\bar{p}/p$ ratios at 1–10 GeV energies, one must divide by the proton spectrum, which cannot be measured directly at those energies because of solar modulation effects. However, we will proceed to quantify the error in the interstellar $\bar{p}/p$ ratio because the uncertainty here concerns the proton spectrum shape, whereas the antiproton flux prediction is sensitive to the proton spectrum normalization.

We focus on two aspects of the spectrum which characterize its shape: the high-energy (>10 GeV) spectral index and the low-energy (<10 GeV) flattening of the spectrum. To determine which spectra will yield the highest and lowest $\bar{p}/p$ ratios in the few GeV range, one just needs to compare the proton fluxes at several GeV with fluxes in the 20–200 GeV range. Spectra with relatively large high-energy fluxes will yield high $\bar{p}/p$ ratios, and spectra with relatively small high-energy fluxes will yield low $\bar{p}/p$ ratios. The proton flux at low energies affects the denominator of the $\bar{p}/p$ ratio. At the measurement energies of several GeV, dividing the antiproton flux by a low proton flux leads to a high $\bar{p}/p$ ratio, and dividing by a high proton flux yields a low $\bar{p}/p$ ratio. The path to designing spectra which extremize the $\bar{p}/p$ ratio is clear: for the maximum $\bar{p}/p$ ratio, we want an interstellar proton spectrum which has a large flux at high energies and a small flux at low energies. The opposite prescription yields the minimum $\bar{p}/p$ ratio.

Since the Golden et al. (1984) data are problematic, let us concentrate on extremizing the $\bar{p}/p$ ratio in the energy range of that data set. To quantify the uncertainty in spectral shape, we start with a parameterization given in Ormes & Protheroe (1983):

$$J_p(R) \propto R^{-\gamma}[1 + (R_0/R)^2]^{-1/2} . \tag{26}$$

To get our $\bar{p}/p$ ratio bounding spectra we pushed the spectral index γ, and the rigidity scale at which the spectrum flattens, R_0, to extreme values. For our upper-bound spectrum we used $\gamma = 2.65$ and $R_0 = 4.7$ GV. For our lower-bound spectrum, we used $\gamma = 2.75$ and $R_0 = 0.47$ GV. In Figure 6 we have plotted the resulting spectra along with the published spectral fits (all renormalized to have the same flux at 8 GeV). These bounding spectra bracket the published fit spectra nicely. In addition, one can fit any of the

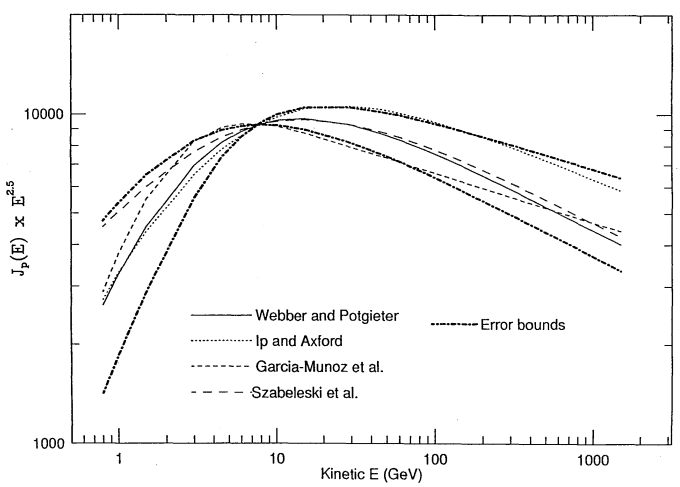

FIG. 6.—Same spectra as in Fig. 2, but here normalized at 8 GeV. Higher $\bar{p}/p$ ratios are found in spectra with the higher fluxes in the 20–200 GeV range. The "bound spectra" are designed to bracket a reasonable range of possible interstellar proton spectra.

data sets in Figure 2 with a spectrum whose shape is within the (ratio) bounding spectra, which also appear in Figure 2 with a different flux normalization to show how they compare with the other spectra.

Calculating the limits on the interstellar $\bar{p}/p$ ratio might seem to be an academic exercise, since solar modulation will be different for the antiprotons and protons. However, during specific periods the amount of solar modulation can be the same for both charge signs. Just such conditions seem to have occurred during the period of the Golden et al. (1984) measurements. In the force field solutions for the modulation of protons and electrons, Perko (1992) finds that the diffusion coefficients have amplitudes which are within 10% of each other, independent of rigidity. Under these conditions one can modulate the $\bar{p}/p$ ratio by merely shifting the energy dependence (Perko 1987). We have done this in Figure 5, and we reemphasize that this test depends on the shape of the proton spectrum and thus is slightly different from the interstellar antiproton flux test in Figure 4. The disagreement with the Golden et al. data is just as strong here as it was in Figure 4.

REFERENCES

Akesson, T., et al. 1982, Phys. Lett., 119, 464
Badhwar, G. D., Daniel, R. R., Cleghorn, T., Golden, R. L., Lacy, J. L., Stephens, S. A., & Zipse, J. E. 1977, Proc. 15th Int. Cosmic Ray Conf., (Plovdiv), 1, 204
Bialas, A., Bleszynski, M., & Czyz, W. 1976, Nucl. Phys. B, 111, 461
Bogomolov, E. A., Krut'kov, S. Yu., Lubyanaya, N. D., Romanov, V. A., Shulakova, M. S., Stepanov, S. V., & Vasileyev, G. I. 1987, Proc 20th Int. Cosmic Ray Conf. (Moscow), 2, 72
Brick, D. H., et al. 1989, Phys. Rev. D, 39, 2484
Cesarsky, C. J. 1987. 20th Int. Cosmic Ray Conf. (Moscow), 8, 87
Cesarsky, C. J., & Ormes, J. F. 1987, in Essays in Space Science (NASA CP-2464)
Engelmann, J. J., et al. 1990, A&A, 233, 96
Faessler, M. A. 1984, Phys. Rep., 115, 1
Ferrando, P., Webber, W. R., Goret, P., Kish, K. C., Schrier, D. A., Soutoul, A., & Testard, O. 1988, Phys. Rev. C, 37, 1490
Gaisser, T. K. 1990, Cosmic Rays (Cambridge: Cambridge Univ. Press)
Gaisser, T. K., & Levy, E. H. 1974, Phys. Rev. D, 10, 1731
Garcia-Munoz, M., Mason, G. M., & Simpson, J. 1975, ApJ, 202, 265
Garcia-Munoz, M., Simpson, J. A., Guzik, T. G., Wefel, J. P., & Margolis, S. H. 1987, ApJS, 64, 269
Ginzburg, V. L., & Ptuskin, V. S. 1976, Rev. Mod. Phys., 48, 161
Golden, R. L., Mauger, B. G., Nunn, S., & Horan, S. 1984, ApJ, 24, L75
Heinbach, U., & Simon, M. 1990, Proc. 21st Int. Cosmic Ray Conf. (Adelaide), 3, 361
Ip, W.-H., & Axford, W. I. 1985, A&A, 149, 7
Krombel, K. E., & Wiedenbeck, M. E. 1987, ApJ, 328, 940
Letaw, J. R., Silberberg, R., & Tsao, D. H. 1983, ApJS, 51, 271
Ormes, J. F., & Protheroe, R. J. 1983, ApJ, 272, 756
Orth, C. D., & Buffington, A. 1976, ApJ, 206, 312
Perko, J. S. 1987, A&A, 184, 119
———. 1992, ApJ, in press
Protheroe, R. J. 1981, ApJ, 251, 387
Ryan, M. J., Ormes, J. F., & Balasubrahmanyan, V. K. 1972, Phys. Rev. Lett., 28, 1985
Salamon, M. H., et al. 1990, ApJ, 349, 78
Seo, E.-S. 1991, Ph.D. thesis, Louisiana State Univ.
Simon, M., Heinbach, U., & Koch, Ch. 1987, ApJ, 320, 699
Simpson, J. A. 1983, Ann. Rev. Nucl. Part. Sci., 33, 323
Smith, L. H., Buffington, A., Smoot, G. F., Alvarez, L. W., & Wahlig, M. A. 1973, ApJ, 180, 987
Soutoul, A., & Ferrando, P. 1989, in AIP Conf. 183, Cosmic Abundances of Matter, ed. C. J. Waddington (New York: AIP), 400
Stephens, S. A., & Golden, R. L. 1987, Space Sci. Rev., 46, 31
Stochai, S. 1990, Ph.D. thesis, Univ. Maryland
Streitmatter, R. E., Stochai, S. J., Ormes, J. F., Golden, R. L., Stephens, S. A., Bowen, T., Moats, A., & Llyod-Evans, J. 1989, Adv. Space Res., 9, 65
Szabeleski, J., Wdowczyk, J., & Wolfendale, A. W. 1980, Nature, 285, 386
Tan, L. C., Mason, G. M., Gloeckler, G., & Ipavich, F. M. 1987, Proc. 20th Int. Cosmic Ray Conf. (Moscow), 2, 239
Tan, L. C., & Ng, L. K. 1983, J. Phys. G, 9, 227
Tuska, E. 1990, Ph.D. thesis, Univ. Delaware
Webber, W. R. 1987, Proc. 20th Int. Cosmic Ray Conf. (Moscow), 2, 80
Webber, W. R., Golden, R. L., & Stephens, S. A. 1987, Proc. 20th Int. Cosmic Ray Conf. (Moscow), 1, 325
Webber, W. R., & Potgieter, M. S. 1989, ApJ, 344, 779